Mechanical Expansion of Thick-Walled Microgroove Tube for High Pressure ACR System

Ding Tang[1]
e-mail: tangding@sjtu.edu.cn

Dayong Li

Yinghong Peng

Zhaohui Du

School of Mechanical Engineering,
State Key Laboratory of Mechanical System and Vibration,
Shanghai Jiao Tong University,
Shanghai 200240, China

This paper presents a study on the expansion process, which joins fins to thick-walled microgroove tubes for high pressure air conditioning and refrigeration (ACR) heat exchanger. Experiments of the tube expansion process have been carried out. An FE model with explicit algorithm is established to study the forming quality of the tube and a novel FE model with implicit algorithm is developed to investigate the local tube-fin joining status. Evaluation of the joining quality along the longitudinal axis of the tube is tried. Both FE and experimental results show that in longitudinal section, tube-fin contact is far from full contact status and internal gaps are observed. Accordingly, process parameters and expanding die geometry are examined. Results show that among the processing factors, the expanding ratio is the major factor influencing the joining status and comprehensively beneficial range of the expanding ratio is discussed.
[DOI: 10.1115/1.4002257]

Keywords: tube expansion, thick-walled, microgroove tube, tube-fin joint

1 Introduction

Tube expansion is a forming process that enlarges the diameter of air condition and refrigeration (ACR) tubes to form tight interferential tube-fin joints as well as thermal bonds. It is widely used in production of tube-fin heat exchanger plate for high efficiency, cost-effectiveness and reliability [1–3]. Efforts have been made to study the expanding forming of normal ACR tubes. Chung et al. [4] studied and optimized the moving velocity of die for tube expanding process in the manufacturing of heat exchangers. Yokell [5] studied the tube expanding process and residual interfacial stress at the tube-hole interface. He proposed a concept of two-stage expanding, which is first applying sufficient pressure or torque to create firm tube-hole contact over a significant part of the fins' thickness and then re-expanding at full pressure or torque. Bariani and Soavi [6] studied contact pressure distribution in circular tube expanding using a conical plug (expanding die).

In recent years, because of the global regulation on hydrochlorofluorocarbons (HCFCs) emission due to its zero ozone depletion characteristics, high pressure (more than 10 MPa) ACR systems using natural refrigerant such as CO_2 have attracted significant attention and are favorably regarded as viable alternatives [7–10]. However, the tubes, which are 3–4 times thicker than normal ones raise difficulties in tube-fin joining process [11]. Moreover, the spiral microgrooves inside the tube for heat exchange enhancement bring extra difficulty in calculating the expansion ratio. Up to now, studies on the expanding of thick-walled ACR tube are lacking. Moreover, in past studies [2,3,5,6] on elastic-plastic expanding theory, tube-fin contact is regarded as a plane strain problem by assuming full contact along axis of the tube but the true contact status is not evaluated.

Consequently, in the present study, expansion processes joining the thick-walled microgroove copper tube to the aluminum fins are investigated. First, forming quality of the tube is studied with both an explicit FE model and a forming experiment. Then, tube-fin joining status is observed with both numerical and experimental methods. The effects of expanding ratio and die geometry are discussed. Suggestions are proposed on improvement of the mechanical and thermal performance by optimizing the process parameters.

2 Forming Quality of the Tube

For high pressure ACR systems, forming quality of the tube relates to the service life. In this section, numerical and experimental methods used to study the factors that influence the tube forming qualities are described.

2.1 Principle of the Forming Process. The schematic illustrating the tube expanding process is shown in Fig. 1. The diameter of the fin hole is slightly larger than that of the expanding die. The collars of the flanged holes allow interval spaces between fins. The ends of the tubes as well as the fins are constrained along the tube's center line. When the die moves forward, the tube undergoes plastic deformation and the "L" shaped collar of the fins is extended by the tube's outer surface. Under designed elastic and plastic deformation for the fin collar and tube, tight fit for a thermal band is obtained. The fit depends on the elastic deformation and springing back of the fin collar. Moreover, structures deformed are quite small in sizes (0.1 mm in fin thickness and 1.5

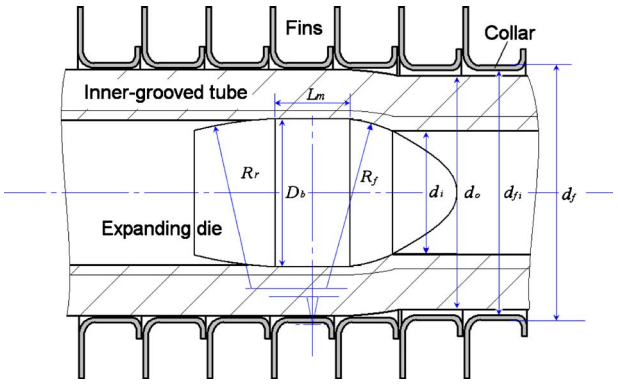

Fig. 1 Tube expanding process

[1]Corresponding author.

Contributed by the Pressure Vessel and Piping Division of ASME for publication in the JOURNAL OF PRESSURE VESSEL TECHNOLOGY. Manuscript received April 26, 2008; final manuscript received July 18, 2010; published online January 31, 2011. Assoc. Editor: L. Ike Ezekoye.

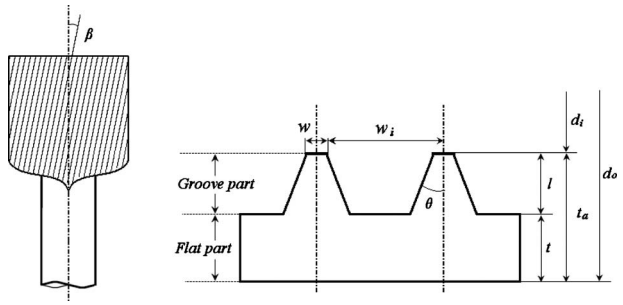

Fig. 2 Groove configuration

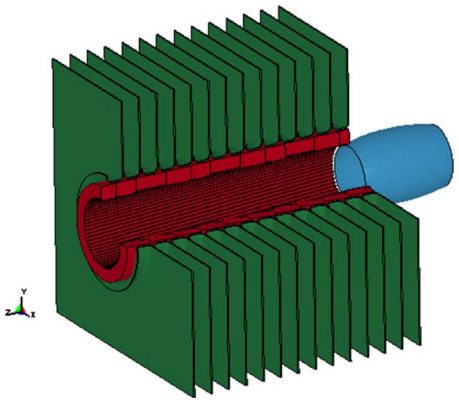

Fig. 3 FE model with explicit algorithm

mm in collar length). Thus, precise elastic-plastic deformation and interactive forces among the various parts is essential. This requires strict control of the expanding die's geometry parameters.

The expanding die is composed of a shank and a bullet, and the geometry parameters are shown in Fig. 1. Key surfaces of the bullet can be divided into three parts. The front part is an arc with radius of R_f, which expands the inner diameter of the tube from d_i to D_b. The middle and rear parts function to iron the internal surface and prevent the tube from overly springing back. The bullet geometry can be described with the parameters D_b, R_f, L_m, and R_r. Among them, D_b relates to the expanding ratio K by the following equation:

$$K = \frac{(D_b - d_i) - (d_{fi} - d_o)}{d_{fi}} \times 100\% \quad (1)$$

in which d_o is outer diameter of the tube and d_f is inner diameter of the fin hole. The groove geometry of interest is a commonly used type as shown in Fig. 2. The configuration parameters used in this study are given in Table 1.

2.2 FE Modeling. As modeling the contact behavior is complex (there are contact pairs of die-tube, tube-fin, and fin-fin), an explicit algorithm is chosen and the commercial FE code LS-DYNA is utilized for its universality. As is shown in Fig. 3 (1/4 of the tube-fin structure is hidden in order to show the inner grooves), three parts are established in the explicit FE model, namely, expanding tool, inner grooved tube, and layers of fins. The inner grooved tube is structured with solid elements with an average size of 0.2 mm while the fins are modeled with shell elements with thickness of 0.1 mm. The tool is assumed as a rigid body. The geometry of the grooves is according to Table 1.

The friction properties between components were taken into account with experimental data. Pin-disk tests were carried out according to ASTM standards (ASTM 1943) for tube-fin friction. However, for the tube-bullet friction, the Pin-disk test with rotational relative motion is inapplicable because the direction of relative movement between bullet and spiral grooves is fixed during the processing. So a device with translational relative movement was developed [12]. According to the test, moving friction coefficients of tube-fin and tube-die are assigned with values of 0.07 and 0.13, respectively.

The materials for the tube and fins are C1220 copper and 1100 aluminum, respectively. For aluminum fins, hardening effects from sheet metal forming is slight and thereby ignored. However, for the copper tubes, hardening is severe due to the embossing process required to make the grooves [13]. Thus, a uniaxial tensile test of the hardened tube was carried out to determine the appropriate stress-strain relationship for modeling purpose. In the FE model, the strain hardening behaviors of both materials are described by Swift's power-law equation [14] as

$$\sigma = k(\varepsilon)^n \quad (2)$$

where k is the strength coefficient and n is the hardening exponent. Table 2 shows the mechanical parameters for the tube and the fins applied in the simulations.

2.3 Experimental Validation. Tube expanding equipment and bullets of the die are shown in Fig. 4(*a*). The expanding die is driven by a hydraulic cylinder. Under the platform, a Kistler piezoquartz dynamometer (with sensitivity of 10mv/N) is used to record the deformation resistances force during tube expanding. At the beginning of the process, the clamp dies hold the tube tightly against each other. Then, the pair of bullets, as shown in Fig. 4(*b*), is pressed into the U-type tube. As the bullets move, the fins have trends of slippage along the center line of the tube. After the bullets move past all the fins, they move back for a reverse expanding. The springing back of the fin collar generates the joining force. The dynamometer records the driving force along the tube's center line during the expanding process, which is an important processing parameter in the design of the hydraulic driving equipment.

As plotted in Fig. 5, comparison of the driving force (deformation resistance force) is shown on both forward and reverse expanding processes from results of experiments and FE models. Explicit numerical results are fairly close to the experiment data in steady value of the expanding force. The difference of the curves at the period beside the steady value is caused by the rigid settings to the die, which have little effects on the steady value. The av-

Table 1 Key seizes of the structures

	Groove configuration	Value
Tube	Outer diameter d_o (mm)	7.00
	Inner diameter d_i (mm)	4.8
	Flat wall thickness t (mm)	0.90
Groove	Groove height l (mm)	0.20
	Tip width w (mm)	0.03
	Apex angle θ (deg)	40
	Helix angle β (deg)	15
	Groove interval width w (mm)	0.37
Fin collar	Outer diameter d_f (mm)	7.30
	Inner diameter d_{fi} (mm)	7.10

Table 2 Mechanical properties

Material parameters	Tube	Fin
Strength coefficient k (MPa)	587	145
Hardening exponent n	0.12	0.13
Young's modulus E (GPa)	112	75
Initial yield stress, σ_s (MPa)	259	90
Poisson's ratio γ	0.30	0.33

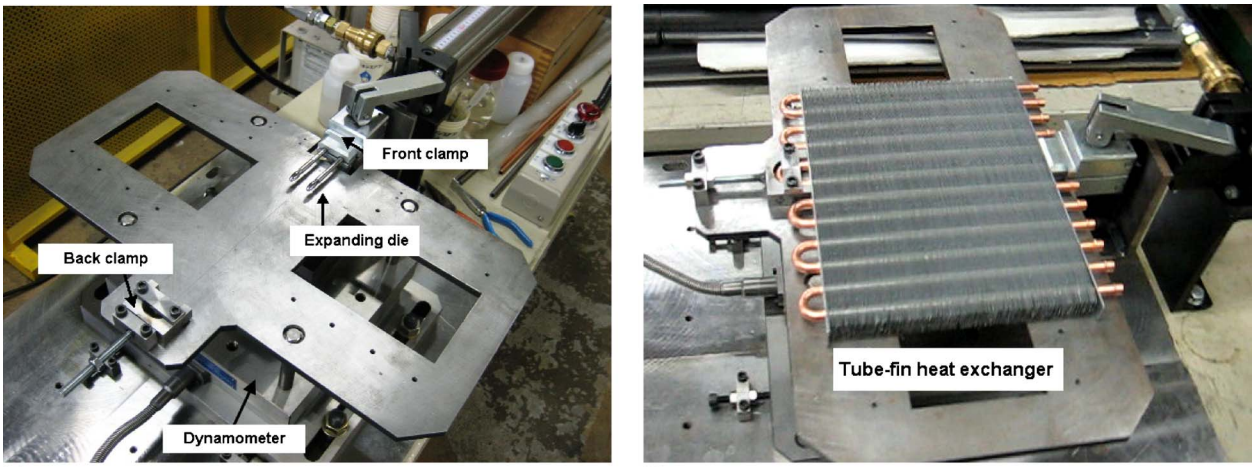

(*a*) (*b*)

Fig. 4 Experiment equipment: (*a*) platform and (*b*) specimen

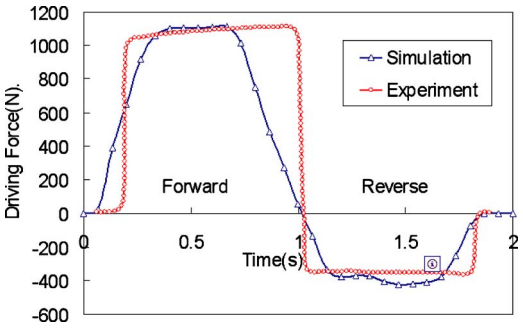

Fig. 5 Varying of driving force in forming process (R_f = 13 mm)

erage difference of the steady value is less than 3%. Wall thickness and groove height of the tube after expansion were measured by optical microscope and compared with the numerical results. The difference was less than 6%.

2.4 Discussions on Forming Quality of the Tube. The reduction of wall thickness and groove height are important factors associated with service life and energy efficiency ratio (EER) performance of the heat exchanger. Influence of the bullet geometry on the service life and the EER performance is examined using the validated FE model. The reduction ratios of the flat wall thickness (ζ_l) and the groove height (ζ_t) were calculated by the following equations, respectively.

$$\zeta_l = [(l - l')/l] \times 100\% \quad \text{(wall thickness)} \tag{3}$$

$$\zeta_t = [(t - t')/t] \times 100\% \quad \text{(groove height)} \tag{4}$$

where l' and t' are the wall thickness and groove height after expanding, respectively.

Simulations were carried out to evaluate the effects of the expanding ratio K and the radius of the die's front part R_f on the reduction ratio while geometry parameters L_m and R_r were set as 1.2 mm and 16 mm, respectively (the geometry parameters are denoted in Fig. 1). Figure 6(*a*) shows the influence of K and R_f on reduction ratio of the wall thickness. With the increasing of the K, the wall thickness reduced linearly with a large slope. Effect of R_f on the wall thinning is not obvious. Figure 6(*b*) shows the influence of K and R_f on reduction ratio of the groove height. The expanding ratio is also the major factor influence on the finished groove height as the larger diameter of the expanding die brings the larger radial pressure on each tooth. With the increase in the R_f, the reduction ratio of the groove height increases at first, then decreases when R_f is over 17 mm.

For the tube expansion process, the driving force on the bullet is an important process parameter. Experimental results found that a large driving force could cause an unevenness of the tube wall thickness by over pushing the metal flow to one end. Figure 7 shows the peak value of the driving force of the forward process under a different set of K and R_f from the result of the explicit model. The increasing of R_f will enlarge both deformation resistant force and friction force so its influence on driving force is obvious.

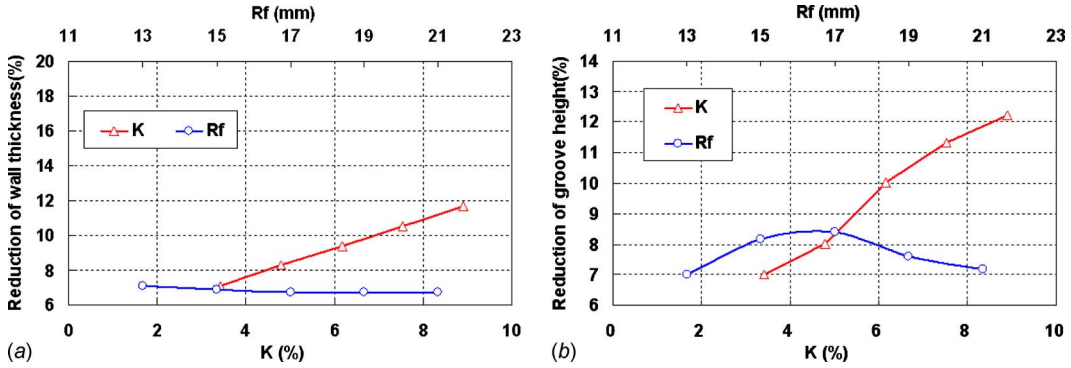

(*a*) (*b*)

Fig. 6 Effect of the K and R_f on forming qualities: (*a*) wall thinning and (*b*) groove height reduction

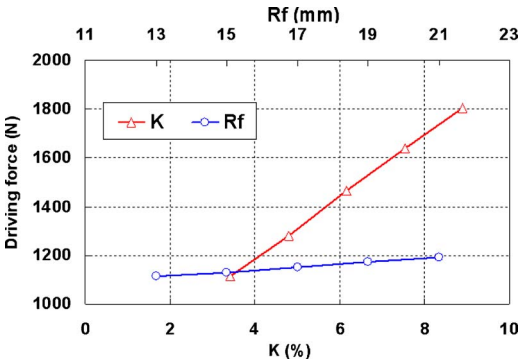

Fig. 7 Effect of the geometry factors on driving force

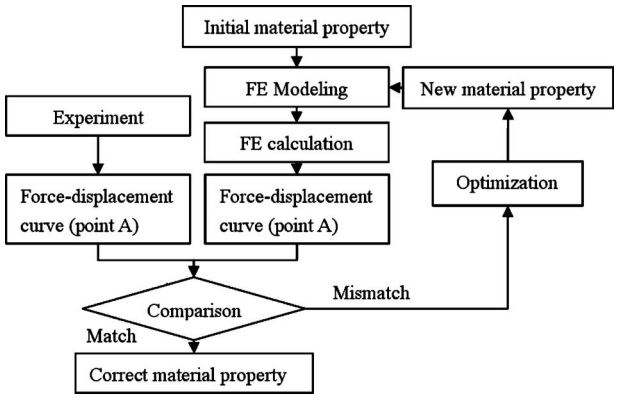

Fig. 9 Flow chart of numerical-experimental method

3 Forming Quality of the Joining Status

As the main purpose of expansion forming, the tube-fin joining quality is the key factor for the processing. However, the joining status has been historically less studied due to the difficulties both in FE simulation and experimental inspection. In this section, innovative FE simulation and experimental inspection techniques are described that were carried out to study the tube-fin joining.

3.1 FE Modeling. The tube-fin joining quality is largely decided by the springback and hooping stress of the fin collar so results of the springback behavior is crucial for the FE simulation. Therefore, implicit algorithm was chosen for the FE modeling for its accuracy in springback calculation. Furthermore, as the joining structures such as the fin collars are very small, an overly fine mesh would cost too much computationally. So in this study, in order to obtain accurate results in joining status, the structure of the inner grooves are all equivalently substituted so that the inner grooved tube can be simplified as an axially symmetric model.

Treatment of the inner grooves was the key part in the FE modeling. In this study, the grooved structure was equivalently substituted by a "soft" layer that is capable of volume compression with the same deformation behavior as the grooved layer inside the tube. The Gurson material model has been widely used to study the deformation of metallic materials containing compressible voids [15]. In compression, the porous material "hardens" due to closing of the voids and in tension, it "softens" due to growth and nucleation of the voids. The Gurson yield function is defined as

$$\Phi\left(\sum_{ij},\sigma_{\text{eq}},f\right)=\left[\frac{\sum_{\text{eq}}}{\sigma_{\text{eq}}}\right]^2+2q_1f^*\cosh\left[\frac{3q_2\sum_m}{2\sigma_{\text{eq}}}\right]-[1+(q_3f^*)^2]=0 \quad (5)$$

where the Σ_{ij} is the macroscopic stress, σ_{eq} is the effective stress of the original material, f is the percent of the cavity volume, Σ_{eq} is the macroscopic effective stress, f^* is the function of f, Σ_m is the macroscopic hydrostatic stress, and q_1, q_2, q_3 are the parameters with consideration of interaction of cavities.

The grooved layer of the tube was substituted with solid layer described by a Gurson constitutive model. In this way, an implicit axial-symmetry model was established as shown in Fig. 8. The tube was modeled as a double layered structure. The Gurson model was applied to the inner layer while a normal elastic-plastic model is applied to the outer layer.

The average size of element for the tubes, fins, and die were 0.05 mm, 0.02 mm, and 0.07 mm, respectively, which are significantly smaller than for the explicit model. A rigid body is assumed for the tool. Key sizes of the geometry model are as same as the explicit model.

3.2 Treatment to the Inner Grooved Layer. As the grooved structure was substituted by a special layer with a Gurson constitutive model, the corresponding material parameters in Eq. (5) were needed for the proper deformation behavior of the grooved structure. In this analysis, a mixed numerical-experimental method was applied in the estimation of the material parameters. Mixed numerical-experimental techniques are frequently used for the characterization of metals with composite or microstructures [16,17].

The methodology of the material parameter estimation is shown in the flow chat of Fig. 9. First, according to the load condition of the grooved layer in tube expansion, a pressing experiment is designed with its schematic shown in Fig. 10. A compression test is done with flattened specimen of the grooved tube on a material testing machine so that a curve showing the relationship between the reaction force and the displacement can be obtained. Then, an optimization process integrates the calculation of the FE model with the inner layer using the Gurson model (Fig. 10). The optimization algorithm keeps providing a new set of material properties until a curve from the simulation results matches the experimental one. In this way, material property of the equivalent layer can be found.

With the material property obtained by the mixed numerical-experimental method, its FE result is compared with that without material property adjustment, as is shown in Fig. 11. It is seen that for the model without material property adjustment, because of the volume incompressibility, the metals are forced to flow toward

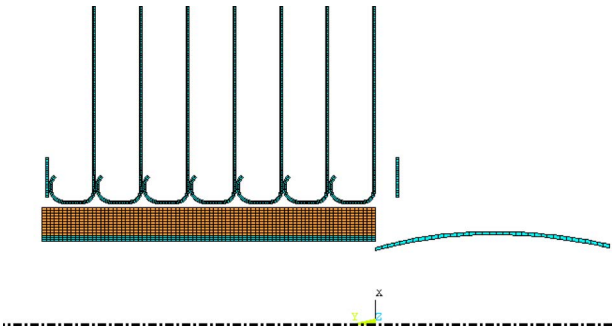

Fig. 8 Axial-symmetry FE model

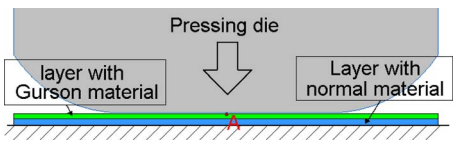

Fig. 10 FE model of the pressing experiment on the material testing machine

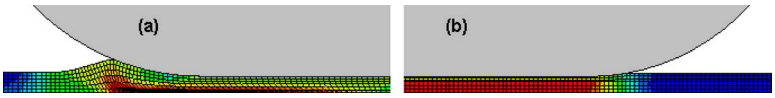

Fig. 11 Comparison of the two FE results: (*a*) upper layer modeled with normal material model and (*b*) upper layer modeled with Gurson material mode

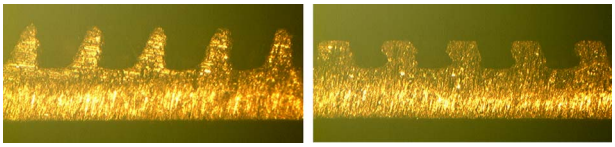

Fig. 12 Section of the grooved layer before and after pressing

both sides. So the deformations of both layers are severe. However, by applying the Gurson model, the deformations of both layers are uniform in lateral direction. Figure 12 shows the section of the flat grooved spacemen before and after the compressing. As the teeth section became wider after the pressing, the groove layer teeth took most part of the deformation in the thickness direction. Results of the FE model with the Gurson material (Fig. 11(*b*)) agree with the experimental results (Fig. 12).

4 Result and Discussion on Joining Quality

In an attempt to understand the complex mechanism of the tube expansion process, the expanding ratio and its effect on the joining quality was examined using both present simulation and experimentation results. Moreover, the influence of the bullet geometry on forming quality is shown.

4.1 Tube-Fin Contact Status. In previous studies, tube-fin joining was frequently regarded as a perfect face-to-face contact due to the difficulties in inspection. However, current simulation results suggest this may not be the case. Figure 13 shows the tube-fin contact status of FE models with expanding ratio setting as 4.79%, 6.16%, and 7.53%. It can be seen that a gap is created between the contact surfaces during the expansion process, and with the increase of the expanding ratio, the height of the gap also increases. The gap can weaken the joint's mechanical strength and also the thermal conductance. The closed gap space isolates the heat transfer contact surfaces to a few points and thereby degrades overall EES performance of the ACR system.

The simulation results of the fin-to-fin pushing stresses with different expanding ratio in Fig. 13 were examined. It is found that they are in the same level (about 10 MPa) so the pushing stress is the not the main reason for the contact status. The gap length and the expanding ratio are directly related.

4.2 Experimental Observation of the Gap. In order to validate the tube-fin joint integrity from FE results, experimental observation is done to examine the tube-fin contact. First, specimens were made with the same expansion ratio as used in the simulation cases. As shown in Fig. 14, the specimens with length of 11 mm were cut through the center line of the tube to expose their axial joint section. Sectional cut of the fin collar will remove the hoop stress and cause springback of the fin collar. In order to observe the original status of the tube-fin contact section, the specimens were inlayed with liquid resin before cutting. After solidification of the resin, the specimens were cut and the exposed sections were polished for observation. Tube-fin contact sections under different expanding ratio are shown in Fig. 15. The trends between contact gap and expansion ratio agree with the experiment results, which show the existence of a gap at the middle of the fin collar, and with the increase in the expanding ratio, the gap height increases.

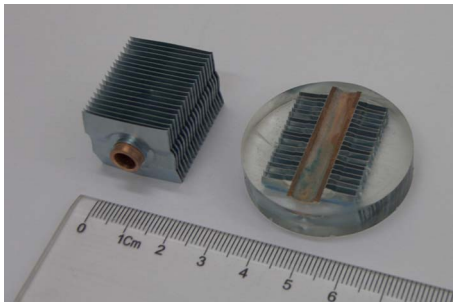

Fig. 14 Preparation of the specimen

4.3 Influence of Expanding Ratio on the Contact Status. Figure 16 presents profiles of the fin collar under different expanding ratios. With the increase of the expanding ratio, the gap height H_g and the gap width W_g increase simultaneously. It means that the fin-to-fin pushing stress along the tube's center line is not essential for the forming mechanism of the gap. From Fig. 16, it can be seen that with the increasing of the expanding ratio, there are trends of metal flow from the sides of the fin collar to the middle part as denoted with arrows. The metal flow is caused by the enlargement of the fin collar's diameter. Therefore, the main reason for the deformation mode of the fin collar and the final fin-tube contact status is the hoop stress of the fin collar.

The tube-fin thermal contact conductance can be evaluated

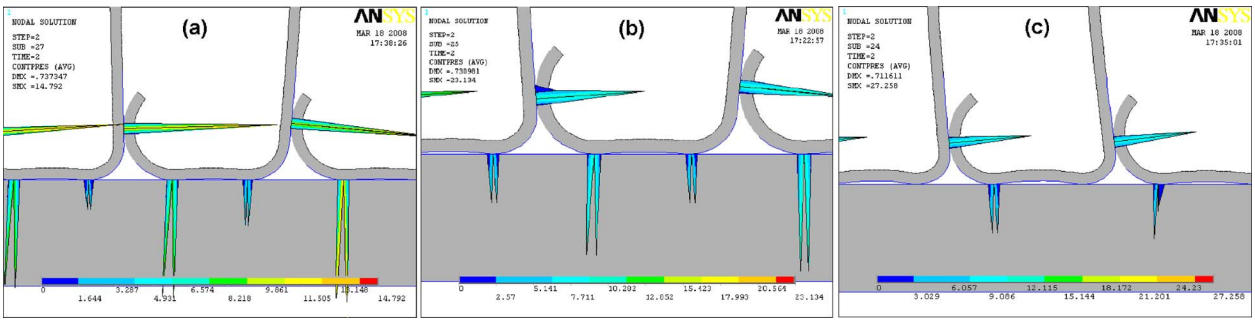

Fig. 13 Fin collar formed at different expanding ratio: (*a*) 4.79%, (*b*) 6.16%, and (*c*) 7.53%.

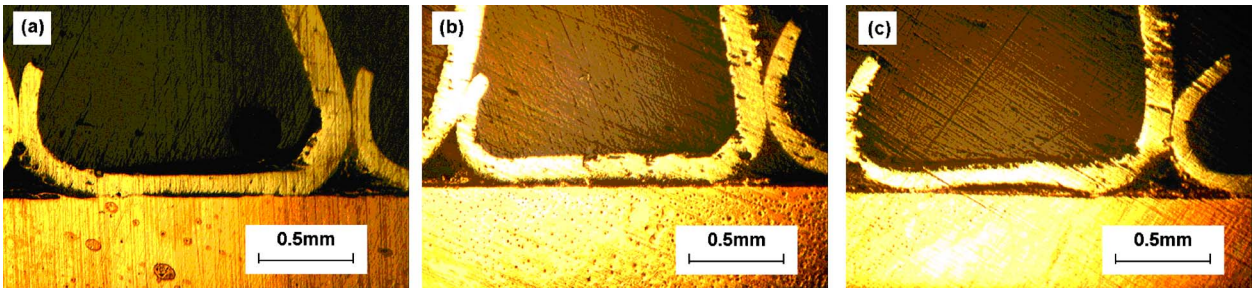

Fig. 15 Fin collar formed at different expanding ratio: (*a*) 4.79%, (*b*) 6.16%, and (*c*) 7.53%

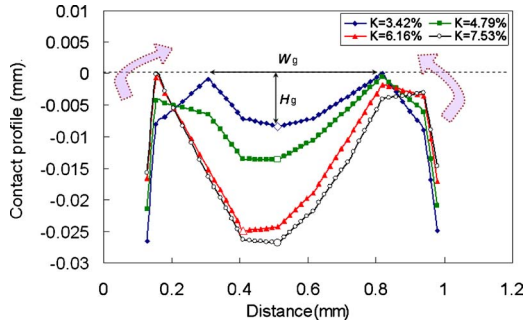

Fig. 16 Comparison of profiles of fin collar's contact surface

from the simulation result of the contact status. For this relationship, the plastic model of Sridhar and Yovanovich [18] and Lambert and Fletcher [19], which is widely used in engineering, was applied.

$$h = 1.25 \cdot \frac{cm}{\sigma} \cdot \left(\frac{P}{H_s}\right)^{0.95} \tag{6}$$

where h is the thermal contact conductance ($W/m^2/K$), c is the average thermal conductivity of the two contact solids (W/m/K), m is the effective slope of surface microprofile, σ is the effective surface roughness (m), P is the contact pressure (Pa), and H_s is the microhardness of the softer surface (Pa). The equation indicates that for the expanding process, h is defined by contact length and pressure. In order to calculate the forming process to thermal performance, the average contact pressure along the tube's center line (in X direction) $\bar{P}$ is defined as

$$\bar{P} = \int_0^L P(x)dx/L \tag{7}$$

where L is the length of middle part of the fin collar with potential of contact (m) and P(x) is the distribution of the contact pressure along the tube's axis (Pa). By definition of $\bar{P}$, the quantified evaluation of the forming quality on thermal performance can be carried on. Distribution of contact pressure along the fin collar under different expanding ratio was obtained from the numerical results as shown in Fig. 17(*a*) from which $\bar{P}$, under different expanding ratios, has been calculated and plotted in Fig. 17(*b*). It indicates that $\bar{P}$ performs better when expansion ratio is between 2% and 6%, which is much larger than that of ACR tubes with normal thickness. The maximum value of $\bar{P}$ is 1.76 MPa when K is 4.79%. After K is over 6%, the magnitude of pressure decreases rapidly due to the large plastic deformation of the flanged hole.

Besides microstructures as fin collar, effects of the expanding ratio are also reflected on overall states such as fin pitch. As fin distribution with uneven spacing affects normal airflow passing through and thereby increasing the thermal resistance, fin pitch is required under limitation. As depicted in Fig. 18, pitch angle increases dramatically when K is over 6%. The reason for the fin pitch is buckling of the fin collar when the stress is in range of material yield.

5 Conclusions

Tube expansion process and factors influencing the forming qualities are studied. Forming quality of the tube is evaluated with wall thinning and reduction of the groove height. Contact status of the tube-fin joint is explored. A novel axial-symmetry implicit FE model was established with the grooved part of the tube substituted with solid part with Gurson constitutive model. Simulation

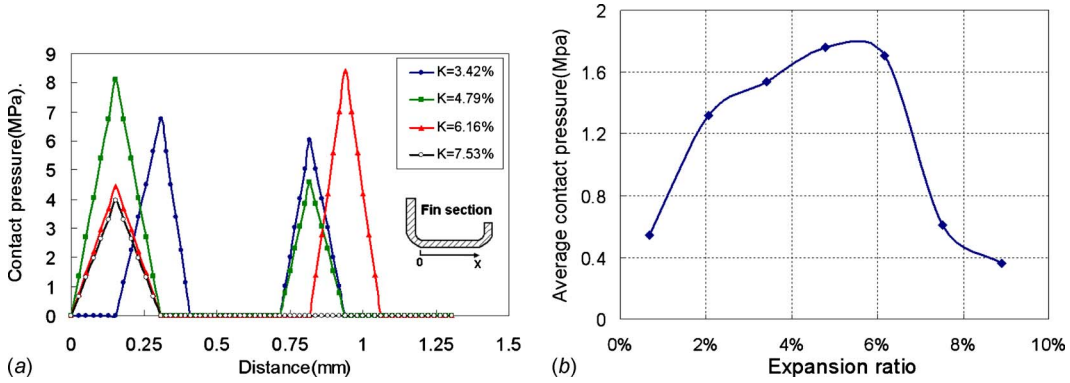

Fig. 17 Contact pressure: (*a*) distribution along the fin section and (*b*) average contact pressure

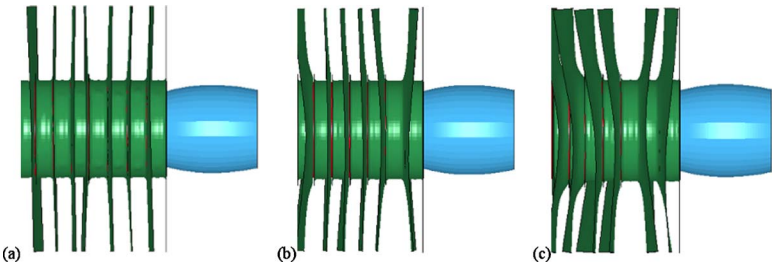

Fig. 18 Effect of expanding ratio on fin pitch: (*a*) *K*=3.42%, (*b*) *K*=6.16%, and (*c*) *K*=7.53%

results on the joining status are validated with the experimental observation with good agreement. Furthermore, roles of the bullet geometry on the forming quality factors, especially the tube-fin joints, have been clemonshated. The following conclusions can be drawn.

(1) The effect of diameter of the expanding die D_b (represented by expanding ratio K) on wall thinning, groove height reduction, and driving force is much larger than other geometry parameters.
(2) The tube-fin joint formed with expanding method is not a facial contact status. Both numerical and experimental results show that joint of the fin collars is far from full contact; a gap is formed between the contact surfaces, which can greatly reduces the thermal conduction.
(3) The expanding ratio is the major factor influencing forming quality of the joint. Parameter $\bar{P}$ is defined as link between forming process and thermal performance. For the thick-walled ACR tube, 2–6% is the recommended safe range for the expansion ratio and $\bar{P}$ can reach 1.76 MPa.

Acknowledgment

The authors would like to acknowledge the financial support of the National Natural Science Foundation of China (Contract Nos. 50634010 and 50821003), the Shanghai Science & Technology Projects (Contract Nos. 09JC1407000 and 1010QH1401400), the Program for New Century Excellent Talents in University (Contract No. NCET-07-0545), and the Shanghai Postdoctoral Sustentation Fund (Contract No. 10R21414300). The authors also appreciate the supported of the Research Fund of State Key Laboratory of MSV, China (Grant No MSV-MS-2010-05).

Nomenclature

D_b = diameter of the die (mm)
R_f = radius of the die's front part (mm)
L_m = length of the die's middle part (mm)
R_r = radius of the die's rear part (mm)
K = expanding ratio (%)
d_o = outer diameter of the tube (mm)
d_i = inner diameter of the tube (mm)
t = flat wall thickness (mm)
ζ_l = reduction ratio of the flat wall thickness (%)
ζ_t = reduction ratio of the groove height (%)
H_g = height of the gap (mm)
W_g = width of the gap (mm)
h = thermal contact conductance ($W/m^2/K$)
L = length of middle part at the fin collar (mm)
P = contact pressure (Pa)
$\bar{P}$ = average contact pressure (Pa)

References

[1] Williams, D. K., 2007, "Comparison of Residual Stresses in the Mechanical Roll Expansion of HX Tubes Into TEMA Grooves," ASME J. Pressure Vessel Technol, **129**(2), pp. 234–241.
[2] Almeida, B. P. P., Alves, M. L., Rosa, P. A. R., Brito, A. G., and Martin, P. A. F., 2006, "Expansion and Reduction of Thin-Walled Tubes Using a Die: Experimental and Theoretical Investigation," Int. J. Mach. Tools Manuf., **46**(12–13), pp. 1643–1652.
[3] Sukhawarn, P., 1970, "Expander Design in the Tube Expanding Process," J. Mech. Eng. Sci., **12**, pp. 30–36.
[4] Chung, W. J., Kim, J. L., Song, T. J., Kim, K. J., and Han, C. M., 2004, "Optimization of Expanding Velocity for a High-Speed Tube Expander Using a Genetic Algorithm With a Neural Network," Proceedings of the IASTED International Conference on Modeling, Simulation and Optimization, pp. 111–116.
[5] Yokell, S., 1992, "Expanded, and Welded-and-Expanded Tube-to-Tube Sheet Joints," ASME J. Pressure Vessel Technol., **114**, pp. 157–165.
[6] Bariani, P., and Soavi, F., 1982, "Contact Pressure Distribution in Circular Tube Expansion Using a Conical Plug," Int. J. Mech. Sci., **24**, pp. 407–424.
[7] Pearson, A., 2005, "Carbon Dioxide—New Uses for an Old Refrigerant," Int. J. Refrig., **28**, pp. 1140–1148.
[8] Wang, R. Z., and Li, Y., 2007, "Perspectives for Natural Working Fluids in China," Int. J. Refrig., **30**, pp. 568–581.
[9] Pettersent, J., Hafner, A., and Skaugen, G., 1998, "Development of Compact Heat Exchangers for CO2 Air-Conditioning Systems," Int. J. Refrig., **21**, pp. 180–193.
[10] Liu, H., 2005, "Experimental Investigation of a CO2 Automotive Air Conditioner," Int. J. Refrig., **28**, pp. 1293–1301.
[11] Friedrich, K., 1999, "Determination of the Optimum High Pressure for Transcritical CO2-Refrigeration Cycles," Int. J. Therm. Sci., **38**, pp. 325–330.
[12] Peng, Y. H., Tang, D., and Li, D. Y., 2008, "Study on the Influence of Mandrel Type on Copper Tube Rotary Draw Bending," Int. J. Mater. Prod. Technol., **32**, pp. 406–422.
[13] Zhang, G. L., Zhang, S. H., Li, B., and Zhang, H., 2007, "Analysis on Folding Defects of Inner Grooved Copper Tubes During Ball Spin Forming," J. Mater. Process. Technol., **184**, pp. 393–400.
[14] Lee, H., Tyne, C. J., and Field, D., 2005, "Finite Element Bending Analysis of Oval Tubes Using Rotary Draw Bender for Hydroforming Applications," J. Mater. Process. Technol., **168**, pp. 327–335.
[15] Wen, J., Huang, Y., Hwang, K. C., Liu, C., and Li, M., 2005, "The Modified Gurson Model Accounting for the Void Size Effect," Int. J. Plast., **21**, pp. 381–395.
[16] Lecompte, D., Smits, A., Sol, H., Vantomme, J., and Hemelrijck, D. V., 2007, "Mixed Numerical-Experimental Technique for Orthotropic Parameter Identification Using Biaxial Tensile Tests on Cruciform Specimens," Int. J. Solids Struct., **44**, pp. 1643–1656.
[17] Meuwissen, M. H. H., Oomens, C. W. J., Baaijens, F. P. T., Petterson, R., and Janssen, J. D., 1998, "Determination of the Elasto-Plastic Properties of Aluminium Using a Mixed Numerical-Experimental Method," J. Mater. Process. Technol., **75**, pp. 204–211.
[18] Sridhar, M. R., and Yovanovich, M. M., 1994, "Review of Elastic and Plastic Contact Conductance Models: Comparison With Experiment," J. Thermophys. Heat Transfer, **8**, pp. 633–640.
[19] Lambert, M. A., and Fletcher, L. S., 1997, "Review of Models for Thermal Contact Conductance of Metals," J. Thermophys. Heat Transfer, **11**, pp. 129–140.